Local- and distant-charge compensation of Eu^{3+} ions in defect centers of $SrTiO_3$

Nigel J. Cockroft* and John C. Wright
Department of Chemistry, University of Wisconsin, Madison, Wisconsin 53706
(Received 1 November 1991)

Site-selective spectroscopy of rare-earth-doped materials has proven to be a powerful method for investigating solid-state defect chemistry at the atomic level. In this paper, the spectral transitions of single-crystal and polycrystalline samples of $SrTiO_3$:Eu^{3+} are sorted by site-selective laser spectroscopy into the major and minor sites that are found in this perovskite-structure material. The major site is shown to have crystal-field multiplicities, relative fluorescence and absorption intensities, level lifetimes, and level degeneracies that are consistent with the tetragonal symmetry associated with a distantly-charge-compensated center. The electronic and vibronic levels for all the visible transitions are determined for this center. These levels exhibit temperature-dependent splittings and shifting that reflects the cubic-tetragonal phase transition that occurs at 106 K. In addition, there are eleven other centers that are assigned to centers with local compensation by vacancies or electronic defects. Electronic defects are also evident from the photobleaching and photoinduced darkening that is also observed in these samples. These effects are observed in both single-crystal and polycrystalline samples, although the linewidths and line shapes of the polycrystalline samples are shown to be dependent on the preparation conditions.

I. INTRODUCTION

This paper is one in a series describing laser-selective excitation (LSE) of trivalent rare-earth ions in perovskite-type materials. We identify 12 Eu^{3+}-ion centers in $SrTiO_3$. The most abundant center was correlated to the center that Weber and Schaufele[1] previously assigned to cubic symmetry for temperatures above 106 K. The greater resolution and sensitivity of LSE allowed the identification of the low-temperature crystal-field splittings of this cubic site. The spectra were consistent with the effect of the cubic-to-tetragonal structural phase transition at 106 K.[2] Nine of the other 11, less abundant, centers were observed in both single crystals and polycrystalline powders. One additional center was found in each of the powders and the single crystal. Most of these centers had lower crystal-field symmetries than the dominant site, indicative of local-charge compensation.

$SrTiO_3$ is a member of the ABO_3 class of perovskite-structure compounds which exhibit a wide range of interesting and useful properties. Such compounds may be ferroelectric,[3] piezoelectric,[4] superconducting,[5] photoconducting,[6] or photochromic.[7] They may also exhibit large dielectric constants,[8] nonlinear optical effects,[9] structural phase transitions,[10] and Jahn-Teller effects.[11] Rare-earth-ion-doped perovskites are particularly useful as positive-temperature-coefficient (PTC) resistors.[12] Most recently, the close structural relatives of these materials have become important high-temperature superconductors.[13]

Many technologically important properties of perovskite-structure materials are intimately dependent on precise control of their defect chemistry. Small variations of stoichiometry, impurity concentration, oxygen fugacity, grain boundaries, and grain sizes typically have a large effect on bulk properties[12,14] because of changes in the perovskite-structure-defect chemistry. The current understanding of perovskite-structure-defect chemistry has been largely inferred from bulk-property measurements. Comprehensive electrical-conductivity studies by Smythe and co-workers[14–17] and Eror and co-workers[18–23] on pure, doped, and nonstoichiometric $SrTiO_3$ provide the basis for current understanding. This work is supplemented by thermogravimetric analysis[24,25] (TGA) and electron-microscopy studies.[3] Whereas bulk measurements may indicate the total numbers of charge carriers or anion and cation vacancies present, they provide no direct observation of microscopic structure. For example, strontium vacancies ($V_{Sr}^{\cdot\cdot}$) (conventional defect notation is used throughout where the subscript describes lattice position of the defect and superscript describes the net charge of the defect) in La^{3+}-doped $SrTiO_3$ can be inferred by TGA studies,[24,25] but the importance of defect association in forming $(La_{Sr}\cdot V_{Sr})'$ centers, etc., can only be determined by techniques that probe the local structure more directly.

Laser-selective excitation spectroscopy is a probe of the local environment of optically active ions.[26,27] The optical ion concentration may be distributed among several centers with different local structure giving complex absorption and fluorescence spectra. However, the spectrum of each center can often be isolated by selective excitation with a tunable dye laser. If the dopant ion is aliovalent, different charge-compensation mechanisms may exist simultaneously. LSE gives relative and absolute quantification of populations of specific microscopic defect centers. Defect equilibria controlling such populations have been successfully studied in a number of doped binary compounds including CaF_2, SrF_2, BaF_2, CdF_2, and PbF_2.[27]

We now report the application of LSE to the more complex tertiary oxides. Whereas previous studies

identified only distant-charge compensation for Eu^{3+} ions on Sr^{2+} sites in $SrTiO_3$,[1,28,29] we provide additional evidence for locally compensated centers. Europium is used as a probe because of the relative simplicity of its spectra.

The importance of local-probe techniques to perovskite-structure materials research has been best illustrated using electron-paramagnetic-resonance (EPR) spectroscopy of transition-metal-doped $BaTiO_3$ and $SrTiO_3$. This work definitively characterized the cubic-to-tetragonal phase transition of $SrTiO_3$ at 106 K as a rotation of oxygen octahedra.[2] Similarly, the local structure of Ti^{4+}-substituted centers of chromium,[10] manganese[11,30–35] and iron[32,33] have been defined by EPR. Rare-earth ions, on the other hand, generally substitute for Sr^{2+} ions. Rimi and Mars[34] determined by EPR that Gd^{3+} substituted for Sr^{2+} in $SrTiO_3$ with distant-charge compensation. They also observed a much weaker signal due to other Gd^{3+} centers, but were unable to resolve or interpret it.

Optical studies in $SrTiO_3$ have been performed with chromium,[35–39] manganese,[36] samarium,[35] and europium[1,28,29] dopants. Each study reports a sole dopant-ion center with distant-charge compensation, but the resolution and sensitivity of previous work may have prevented observation of less abundant centers. The spectrum of $SrTiO_3$:Eu^{3+} has been used to identify the important transitions[1,29] and the vibronic sidebands associated with the major site[1] as well as the nonradiative quenching mechanism.[28] We complement these papers by determining vibronics at lower temperatures and frequencies and the spectral changes that occur from the tetragonal distortion as the temperature is lowered below the 106-K phase transition. In addition, we report 11 locally compensated centers that are also present in Eu^{3+}:$SrTiO_3$.

II. EXPERIMENTAL TECHNIQUES

A flame-fusion-grown single crystal of $SrTiO_3$ doped with 0.01 mol% Eu^{3+} was obtained from Commercial Crystal Laboratories Inc., Naples, FL. Polycrystalline powders of $SrTiO_3$ doped with 0.01%–0.2 mol% Eu^{3+} were prepared by a modified Pechini[40] liquid-mix technique similar to that described by Chau, Sharma, and Smythe.[17] In this method stoichiometric quantities of $SrCO_3$ (Spex 99.999%) powder, Eu^{3+} solution, and Ti^{4+} solution were heated until they polymerized. The mix was typically calcined at 900 °C for 3 h and sintered as a pellet for 16–24 h at 1450 °C. The materials used for solution preparation were tetra-isopropyl orthotitanate [obtained from both Aldrich Chem Co and duPont (Tyzor TPT)], Eu_2O_3 (Spex 99.99%), ethylene glycol (Baker analyzed reagent), and citric acid (Baker analyzed reagent). Powder quality and phase purity were verified by x-ray diffraction on a Nicolet I2/V diffractometer.

A nitrogen-laser-pumped tunable dye laser was used as the excitation source. It had a bandwidth of 0.8 cm^{-1} and pulse width of 10 nsec. The Eu^{3+} transitions between $^7F_0 \rightarrow {}^5D_0$, $^5D_1$, and $^5D_2$ manifolds were excited using Rhodamine 6G, Coumarin 481, and Coumarin 102 dyes (Exciton), respectively. Total fluorescence excitation spectra were recorded by scanning the dye laser while monitoring fluorescence with a 1P28A photomultiplier tube (PMT) on a Jarrell Ash $\frac{1}{4}$-m monochrometer set to zero order. Laser scatter was eliminated by a mechanical rotary chopper at the entrance slit. Low-resolution spectra were obtained using the $\frac{1}{4}$-m monochrometer set to a desired wavelength. Site-selective excitation and fluorescence spectra were recorded using an Interactive Technology 1-m monochrometer with a 1200-lines/mm holographic grating and a dry-ice-cooled EMI 9658R photomultiplier. Near-ir spectra were recorded using an RCA C31034A tube. Excitation and fluorescence signals were recorded with a gated integrator. A gate delay and width of 250/750 μsec for $^5D_0$ and 50/150 μsec for $^5D_1$ fluorescence was used for most centers. Temporal transients were recorded on a LeCroy TR18 transient recorder with data acquisition on an IBM PC/AT microcomputer. Fluorescence wavelengths were calibrated against a Fe-Ne hollow cathode lamp, while excitation wavelengths were calibrated against the optogalvanic spectra obtained with the same lamp. The wavelength accuracy is $\simeq 0.02$ nm, while the precision is $\simeq 0.003$ nm.

Sample temperatures between 12 and 120 K were obtained using a variable-temperature closed-cycle refrigerator (Air Products Displex 1R02W). Polycrystalline powder samples were pressed into 5-mm-diam holes on a copper sample block. The excitation laser beam was focused to a 5 mm$\times$200 μm line on the sample with fluorescence being imaged from this line source. An electromagnet with controllable field strength up to 24 kG was used to verify the degeneracy of the $^5D_1$ and $^5D_2$ levels of the dominant center. Optical absorption was measured with a current-controlled tungsten source and an 0.85-m double monochrometer.

III. RESULTS

A. Single crystal

1. *Absorption measurements*

Optical-absorption spectra were recorded for the $^7F_0 \rightarrow {}^5D_0$ and $^7F_0 \rightarrow {}^5D_1$ regions of Eu^{3+} in the $SrTiO_3$ single crystal at 2.5 K over a path length of 14.2 mm. The only observable peak was a $^7F_0 \rightarrow {}^5D_1$ transition at 526.14$\pm$0.03 nm, which had an absorbance of $(6.9\pm1.0)\times10^{-3}$ cm^{-1}. Peaks with absorbances less than 1.0×10^{-3} cm^{-1} could not be observed. Lamp instability was the primary noise source limiting resolution of weaker peaks. The observed transition is assigned to the $Z1 \rightarrow B1$ transition of the $a1$ center described in more detail in the next section. This center was previously observed by Weber and Schaufele.[1] The absorption spectra were also studied to ensure the absence of accidental contamination from other rare earths or large concentrations of centers where quenching would prevent detection by fluorescence measurement (e.g., centers containing H_2O, H^-, or transition-metal ions). In addition, Fourier-transform infrared-absorption spectra were mea-

sured from 500 to 4000 cm^{-1} to ensure the absence of the OH^- stretching transition at 3495 cm^{-1} in our crystal.

2. *Total fluorescence excitation spectroscopy*

Total fluorescence excitation spectroscopy provided considerably greater sensitivity than optical-absorption measurements. Figures 1, 2, and 3 show the 12-K excitation spectra for $^7F_0 \rightarrow {}^5D_1$, $^5D_0$, and $^5D_2$ transitions, respectively. These spectra were recorded with a 750-μsec-wide gate delayed 200 μsec with respect to the laser pulse. This gate value was somewhat shorter than the 1.05-msec lifetime of the longest-lived site fluorescence, and so there is some enhancement of the shorter-lifetime sites by this choice. The minimum delay was limited by the rotation rate of the chopper used to eliminate laser scatter.

At low temperatures each Eu^{3+} center with a distinct crystallographic environment may exhibit a maximum of one, three, or five pure electronic transitions for excitation to $^5D_0$, $^5D_1$, and $^5D_2$, respectively. Centers of high symmetry have fewer transitions. The large number of transitions in the expanded plots of Figs. 1–3 demonstrate the occurrence of multiple Eu^{3+} centers in this material. The spectral peaks are labeled according to the center assignments inferred from site-selective-spectroscopy experiments described below.

Although the $^7F_0 \rightarrow {}^5D_0$ spectrum is intrinsically the simplest, the $^7F_0 \rightarrow {}^5D_1$ spectra proved the most useful because, unlike $^7F_0 \rightarrow {}^5D_0$, transitions due to cubic-symmetry centers are allowed by a magnetic dipole mechanism. The most intense peak in the total fluorescence $^7F_0 \rightarrow {}^5D_1$ excitation spectra (Fig. 1) corresponds to the single transition at 526.14 nm observed in the absorption spectrum. The peak intensity in Fig. 1(a) is 30 times the peak intensity of the $^7F_0 \rightarrow {}^5D_0$ excitation spectrum [Fig. 2(a)] and approximately 14 times more intense than the strongest transitions due to the other centers in the $^5D_1$ spectrum with the gate and delay values chosen.

3. *Site-selective spectroscopy*

Previous defect chemistry studies of Eu^{3+}-doped materials have demonstrated that the $^7F_0 \rightarrow {}^5D_1$ spectrum is the most useful for monitoring concentrations of centers of various symmetry.[27] We therefore emphasized the unraveling of the $^7F_0 \rightarrow {}^5D_1$ spectrum. Each transition in Fig. 1 was selectively excited with the tunable dye laser and the fluorescence spectra were recorded. The $^5D_0 \rightarrow {}^7F_1$ and $^5D_0 \rightarrow {}^7F_2$ fluorescence transitions were typically the most intense. As expected, several groups of $^7F_0 \rightarrow {}^5D_1$ excitation transitions revealed the same fluorescence spectra. The dominant line in each distinct fluorescence spectrum was then selectively monitored with the 1-m monochrometer. Scanning the dye laser across the $^7F_0 \rightarrow {}^5D_1$ region then gave the site-selective spectrum for each site (Fig. 4). In all cases these excitation spectra were confirmed by monitoring a second fluorescence transition and in some cases a third or fourth transition.

Once the centers were distinguished in the $^7F_0 \rightarrow {}^5D_1$ spectra, the corresponding $^7F_0 \rightarrow {}^5D_0$ transitions were determined by site-selective excitation (Fig. 2). The search for confirmation of the $^7F_0 \rightarrow {}^5D_2$ transitions was less successful in several cases because of their greater numbers and often weaker intensity (Fig. 3).

The site-labeling nomenclature has no physical significance. The dominant center has been labeled $a1$ for consistency with a related report,[41] to appear elsewhere, in which we label the dominant center for each Sr-Ti-O phase by ai, where the i denotes the Sr stoichiometry (i.e., $a1$, $a2$, and $a3$ represent the dominant centers in $SrTiO_3$, Sr_2TiO_4, and $Sr_3Ti_2O_7$, respectively). The additional Eu^{3+} centers in $SrTiO_3$, reported here, are arbitrarily labeled $b-l$.

Where required, specific transitions are labeled using Dieke's empirical spectroscopic notation.[42] Crystal-field levels in $^7F_0, ^7F_1, \ldots, ^7F_6$ manifolds are labeled

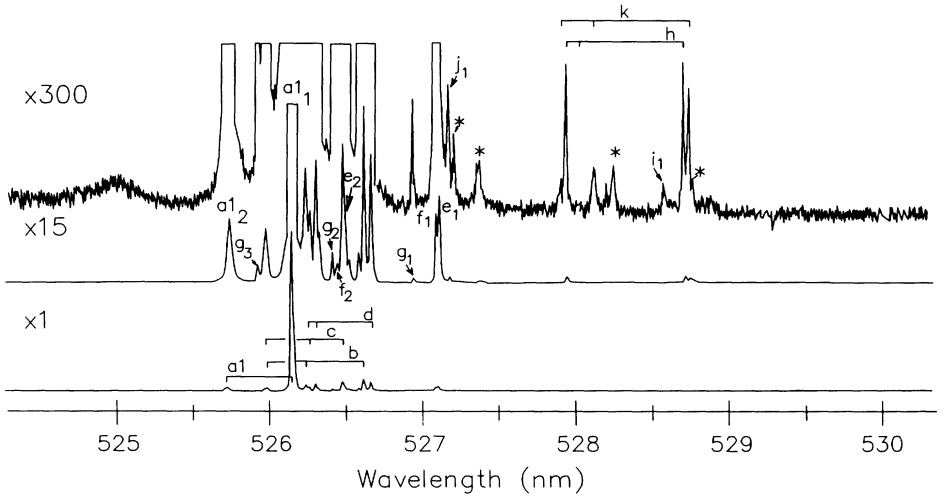

FIG. 1. $^7F_0 \rightarrow {}^5D_1$ excitation spectra (single crystal) monitoring total fluorescence with a temporal gate delay and width of 200 μsec/750 μsec. Labels indicate site and energy-level assignments, while the asterisk indicates unassigned transitions.

$Z_i, Y_i, \ldots, T_i$, while levels in $^5D_0$, $^5D_1$, and $^5D_2$ are labeled A_i, B_i, and C_i, respectively. The subscript indicates the position, within the manifold, of each level in ascending energy order. For the $a1$ center, where the site symmetry and some of the crystal-field state's symmetries are known, the symmetry is labeled using the group representation, i.e., $A1$, $B2$, etc.

a. a1 center. Laser excitation of the strong 526.14-nm transition (Fig. 1) results in intense fluorescence visible to the naked eye. The resultant $^5D_1 \rightarrow {}^7F_{1,2,\ldots,6}$ and $^5D_0 \rightarrow {}^7F_{0,1,\ldots,6}$ fluorescence spectra were recorded. Like other Eu^{3+} studies, spectral overlap of fluorescence from $^5D_0$ and $^5D_1$ to different $^7F_1$ manifolds occurred. The greatest problem was overlap between the following pairs of spectra: (a) $^5D_0 \rightarrow {}^7F_0$ and $^5D_1 \rightarrow {}^7F_3$, (b) $^5D_0 \rightarrow {}^7F_1$ and $^5D_1 \rightarrow {}^7F_3$, and (c) $^5D_0 \rightarrow {}^7F_2$ and $^5D_1 \rightarrow {}^7F_4$. In each of these cases, the desired spectrum was selectively enhanced by changing the temporal gate for photon detection. Emission from $^5D_0$ (typical lifetime of 1.05 msec) was enhanced with respect to $^5D_1$ (typical lifetime of 115 μsec) by using a gate delay of 250 μsec and width 750 μsec. A 50-μsec gate delay and 150-μsec gate width enhanced $^5D_1$ fluorescence. Fluorescence spectra from both the $^5D_0$ and $^5D_1$ states to both the $^7F_1$ and $^7F_2$ states of the $a1$ center are included in Fig. 5.

In addition to the pure electronic transitions, we assigned several vibronic transitions. A detailed examination of expanded-scale spectra at 12 K identified nine vibrational energies, which are summarized in Table I along with their parent electronic transitions. The criteria used for assigning a vibronic nature to the transitions included (a) more transitions than expected for manifold multiplicity, (b) significantly broader linewidths than other transitions in spectra, (c) the appearance of consistent vibronic intervals in many spectra, and (d) the occurrence of anti-Stokes peaks with the same intervals for some spectra. The temperature dependence of the rel-

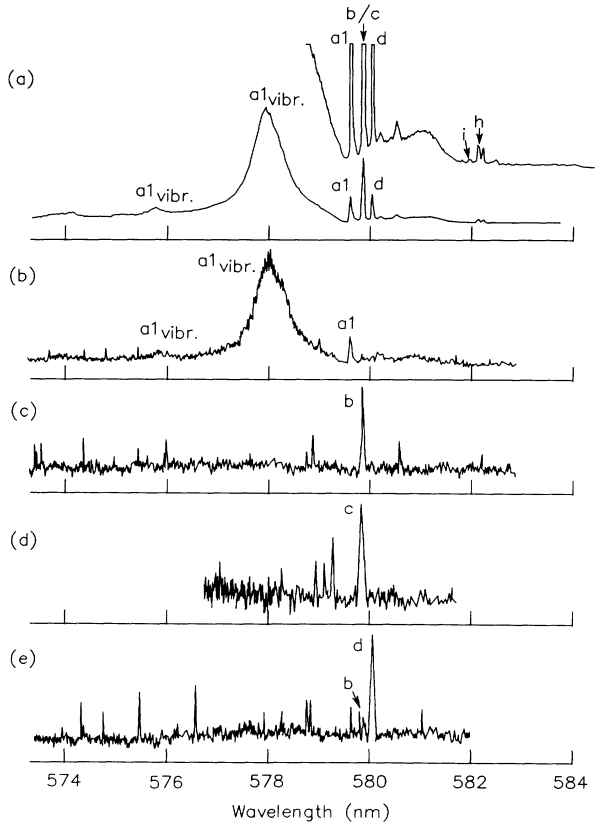

FIG. 2. $^7F_0 \rightarrow {}^5D_0$ excitation spectra (single crystal) monitoring (a) total Eu^{3+} fluorescence, (b) $a1$-center fluorescence at 615.418 nm, (c) b-center fluorescence at 613.435 nm, (d) c-center fluorescence at 613.000 nm, and (e) d-center fluorescence at 613.980 nm.

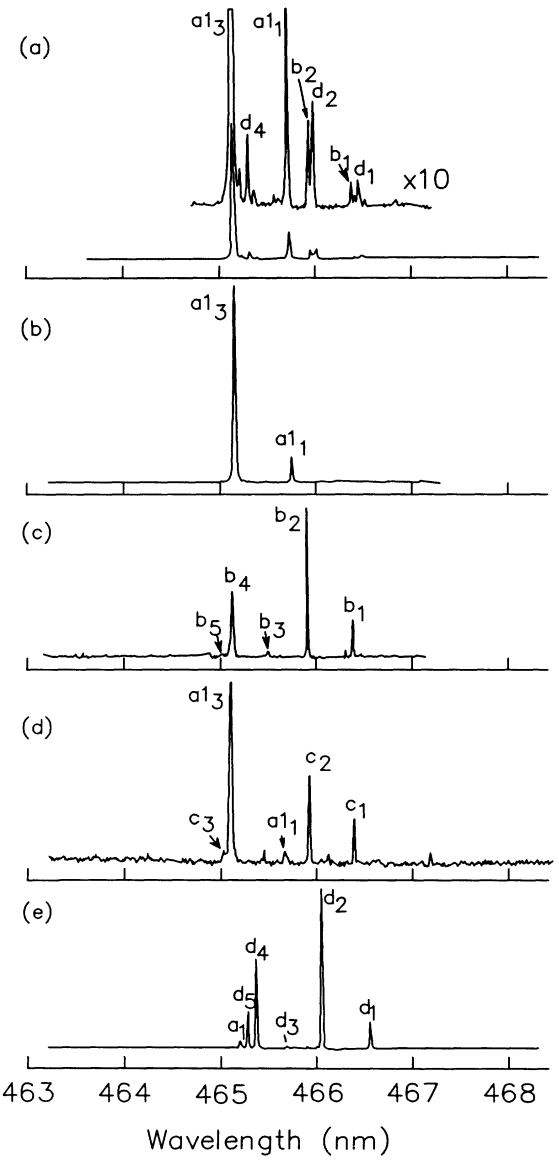

FIG. 3. $^7F_0 \rightarrow {}^5D_2$ excitation spectra (single crystal) monitoring (a) total Eu^{3+} fluorescence, (b) $a1$-center fluorescence at 615.418 nm, (c) b-center fluorescence at 589.795 nm, (d) c-center fluorescence at 591.220 nm, and (e) d-center fluorescence at 590.430 nm.

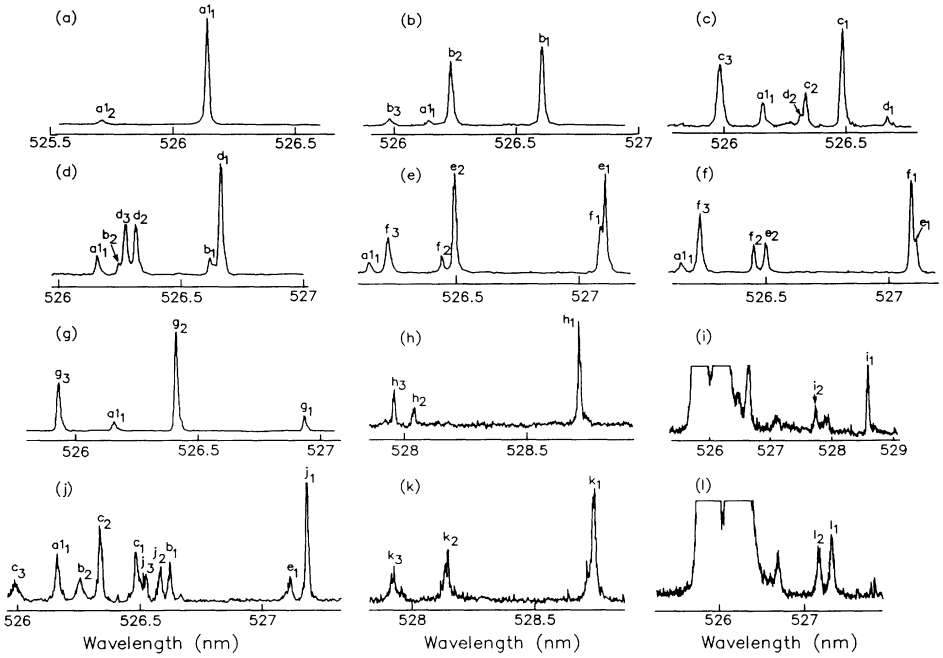

FIG. 4. Site-selective $^7F_0 \rightarrow {}^5D_1$ excitation spectra (single crystal) monitoring the following dominant fluorescence transitions for the $SrTiO_3$:Eu^{3+} sites: (a) 590.901 nm of $a1$ site, (b) 589.795 nm of b site, (c) 590.20 nm of c site, (d) 613.98 nm of d site, (e) 589.44 nm of e site, (f) 589.40 nm of f site, (g) 589.055 nm of g site, (h) 591.385 nm of h site, (i) 618.730 nm of i site, (j) 612.610 nm of j site, (k) 591.500 nm of k site, and (l) 590.585 nm of l site. Line assignments are shown for individual transitions.

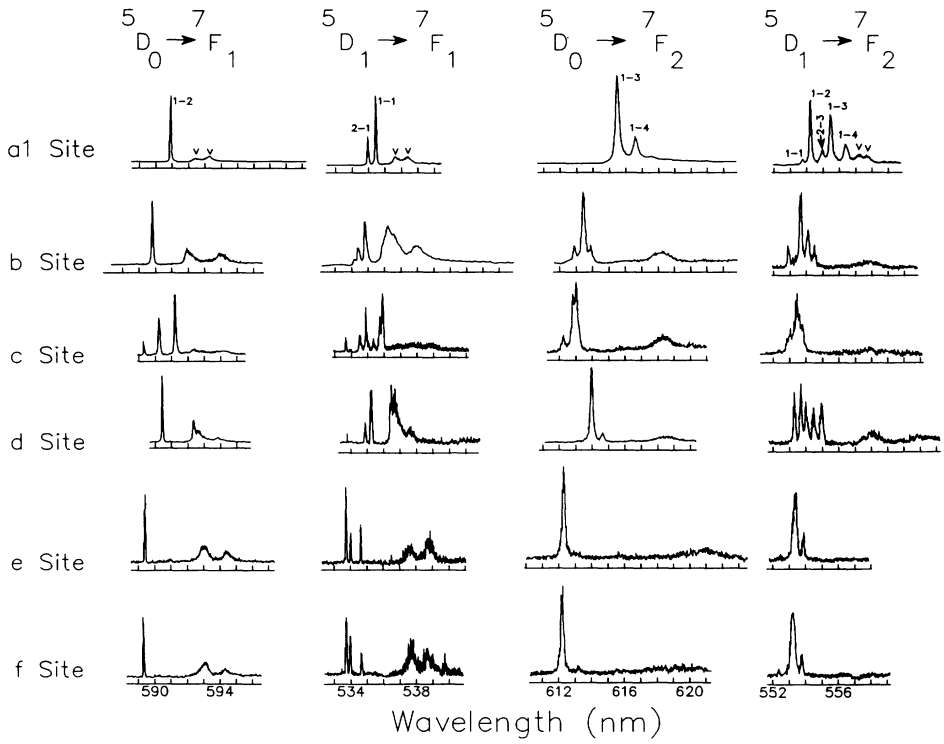

FIG. 5. Fluorescence spectra for $a1$–f sites (single crystal) for indicated transitions. Each of the sites was excited at the $Z_1 \rightarrow B_1$ transition of that site (see Fig. 1 and Table III for the relative line positions).

ative intensities was not used as a criteria because of complications from broadening, line shifting from the phase transition described earlier, and loss of site selectivity in the excitation from overlapping lines.

Weber and Schaufele[28] assigned several Eu^{3+} vibronic energies from the 77-K spectra. We tentatively correlate their modes labeled ν_b (55–60 cm^{-1}), ν_c (120 cm^{-1}), ν_d (170 cm^{-1}), and ν_f (460 cm^{-1}) to our vibrations (see Table I) centered around 56, 116, 182, and 458 cm^{-1}, respectively. Figure 5(a) shows an example of transitions with vibronic states (labeled by v) separated by 42.8 and 63 cm^{-1} from the parent transitions in the $^5D_0 \rightarrow {}^7F_1$ spectrum. These same intervals are seen in many of the spectra. The linewidths of these two vibronic transitions are 0.48 and 0.44 nm, about 6 times larger than the zero-phonon line (ZPL).

TABLE I. Vibrational energies derived from vibronic transitions in the a 1-site excitation and emission spectra at 12 K. The asterisk denotes an anti-Stokes vibronic transition.

Energy (cm^{-1})	Spectrum	Parent electronic transition
30.7	$^5D_0 \rightarrow {}^7F_4$	1-1
30.7	$^5D_1 \rightarrow {}^7F_4$	1-1
41.0	$^5D_0 \rightarrow {}^7F_0$	1-1
42.5*	$^5D_0 \rightarrow {}^7F_0$	1-1
41.0	$^7F_0 \rightarrow {}^5D_0$	1-1
39.5*	$^7F_0 \rightarrow {}^5D_0$	1-1
42.8	$^5D_0 \rightarrow {}^7F_1$	1-2
42.9	$^5D_1 \rightarrow {}^7F_1$	1-1
43.2	$^5D_1 \rightarrow {}^7F_2$	1-4
42.7	$^5D_1 \rightarrow {}^7F_4$	1-7
42.6	$^5D_1 \rightarrow {}^7F_5$	1-2
49.0	$^5D_0 \rightarrow {}^7F_0$	1-1
49.0	$^7F_0 \rightarrow {}^5D_0$	1-1
50.5	$^5D_1 \rightarrow {}^7F_3$	1-4
57.0	$^5D_0 \rightarrow {}^7F_2$	1-3
55.6	$^5D_1 \rightarrow {}^7F_2$	1-3
56.9	$^5D_1 \rightarrow {}^7F_3$	1-5
56.9	$^5D_0 \rightarrow {}^7F_5$	1-2
67.5	$^5D_0 \rightarrow {}^7F_1$	1-2
66.7	$^5D_1 \rightarrow {}^7F_1$	1-1
66.8	$^5D_1 \rightarrow {}^7F_3$	1-4
78.0	$^5D_0 \rightarrow {}^7F_0$	1-1
78.8	$^5D_0 \rightarrow {}^7F_2$	1-3
116.0	$^5D_0 \rightarrow {}^7F_0$	1-1
117.0	$^7F_0 \rightarrow {}^5D_0$	1-1
116.6	$^5D_0 \rightarrow {}^7F_1$	1-2
108.8	$^5D_0 \rightarrow {}^7F_3$	1-4
185.0	$^5D_0 \rightarrow {}^7F_1$	1-2
182.0	$^5D_0 \rightarrow {}^7F_2$	1-3
459.0	$^5D_0 \rightarrow {}^7F_1$	1-2
458.0	$^5D_0 \rightarrow {}^7F_2$	1-3

The peak heights of the $^5D_0 \rightarrow {}^7F_0$ fluorescence spectrum were a factor of 250 weaker than the $^5D_0 \rightarrow {}^7F_1$ spectrum. The single $^5D_0 \rightarrow {}^7F_0$ ZPL at 579.61 nm is very weak compared with the broader, more intense lines at higher and lower energy than are Stokes and anti-Stokes vibronic transitions (Table I) associated with the ZPL.

Unusually low vibronic frequencies were determined from the $^5D_1 \rightarrow {}^7F_0$ fluorescence spectrum when excited by the $^7F_0 \rightarrow {}^5D_2$ transitions. Figure 6 shows a series of sharp but weak lines that appear as fine structure in this spectrum. Since only two pure electronic transitions are expected in this spectrum (with wavelengths consistent with the $^7F_0 \rightarrow {}^5D_1$ excitation spectrum), the remaining lines are assigned to vibronic transitions with intervals 3.3, 7.0, 9.6, 12.6, and 17.6 cm^{-1}. These vibronics were resolved in this spectrum, but not in other spectra, because the unusually narrow-linewidth ZPL's (0.018 and 0.027 nm) allow their resolution.

Any of the fluorescence transitions may be monitored to produce a site-selective excitation spectrum. However, interference from other centers is minimized by monitoring the most intense, narrow-band fluorescence transitions. The optimum transitions to monitor were 590.901 nm ($^5D_0 \rightarrow {}^7F_1$) and 615.418 nm ($^5D_0 \rightarrow {}^7F_2$). Each of these was used to confirm the $^7F_0 \rightarrow {}^5D_0$, $^5D_1$, and $^5D_2$ site-selective excitation spectra for this site given in Figs. 2, 4, and 3, respectively. The multiplicity of the Eu^{3+} crystal-field manifolds is consistent with a tetragonal point symmetry.

Correlation of the electronic transitions in all fluorescence and excitation spectra enabled the derivation of the energy-level scheme of Table II for this center at 12 K. This table augments the measurements in previous work[41] and updates the assignments by the improved understanding of the vibronic transitions. Special emphasis was placed on determining the crystal-field levels of $^7F_1$. All other a 1-center manifolds exhibited multiplicity at 12 K consistent with the expected tetragonal symmetry and inconsistent with cubic symmetry. The $^5D_0 \rightarrow {}^7F_1$, $^5D_1 \rightarrow {}^7F_1$, and $^5D_2 \rightarrow {}^7F_1$ fluorescence spectra and $^7F_1 \rightarrow {}^5D_0$ excitation spectrum, however, all had electronic transitions to or from $^7F_1$ levels of approximately the same energy. Only a cubic-symmetry center can have a single triply degenerate $^7F_1$ manifold. Careful calibration of approximately 40 spectra revealed that the $^7F_1$ levels derived from $^5D_0$ and $^5D_1$ fluorescence were not, in fact, identical within experimental uncertainty. The two distinct levels are split by 0.4 cm^{-1} (Table II).

The observation of two $^5D_1$ transitions in excitation spectra suggests that one level is doubly degenerate. A variable magnetic field was applied to the sample, and the 12-K excitation spectrum of $^7F_0 \rightarrow {}^5D_1$ was recorded. The lower-energy level (19001.1 cm^{-1}) was observed to split with the splitting magnitude $\Delta E = gH$, where $g = 0.037$ cm^{-1}/kG.

Similarly the a 1-center $^7F_1 \rightarrow {}^5D_2$ excitation spectrum was recorded as a function of applied magnetic field. The level at 465.15 nm was found to split, confirming its double degeneracy. There is also an extremely weak line at

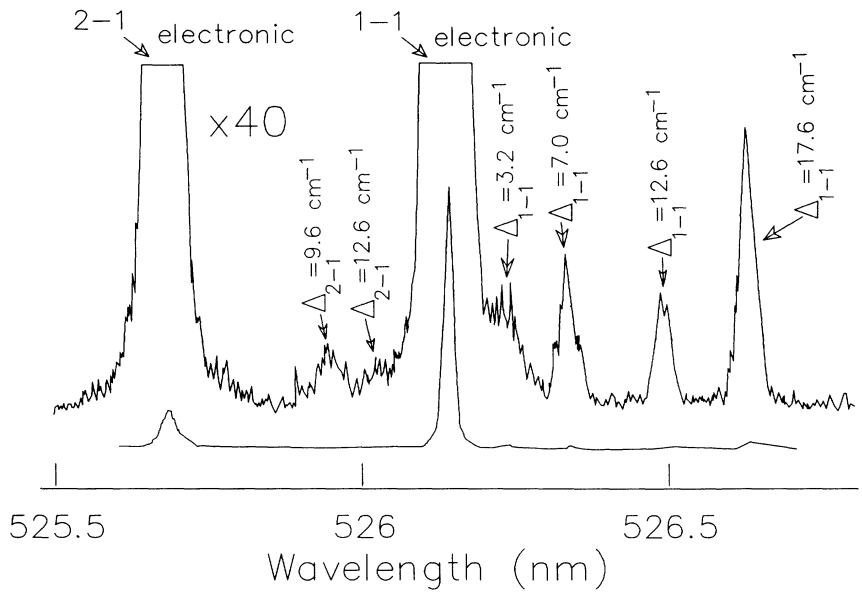

FIG. 6. a1-center $^5D_1 \rightarrow {}^7F_0$ fluorescence after excitation of the a1-center $^7F_0 \rightarrow {}^5D_2$ transition. The vibronic peaks are labeled by the shift (Δ_{i-j}) from the $B_i \rightarrow Z_j$ ZPL electronic transition.

465.59 nm that is assigned to the a1-site $^5D_2$ state at 21472 cm^{-1}. The transition becomes much stronger in the presence of the magnetic field. Hot band emission is also observed from this level.

The position and number of the transitions in this material changes as a function of temperature between 120 and 12 K as is shown in Fig. 7. The two lower-temperature $^7F_0 \rightarrow {}^5D_1$ excitation transitions of the a1 site shift continuously with temperature changes until they collapse to a single transition at 106 K. Explanation of this effect is given in the Sec. IV. This temperature dependence required that the sample temperature be measured for each experiment in order to achieve reproducible spectra. The temperature was reproduced by measuring the $^5D_1$-level separation since the changing energy-level separation invalidated using Boltzmann population factors.

The lifetime of the $^5D_0$ level could not be measured by direct excitation because of the weak $^7F_0 \rightarrow {}^5D_0$ absorption strength. Instead, the $^5D_1$ and $^5D_0$ fluorescence transient was measured after excitation of the $^7F_0 \rightarrow {}^5D_1$ transition. The single-exponential decay of the $^5D_1$ level had a lifetime of 136 μsec, while the decay of the $^5D_0$ fluorescence could be fit with two levels having lifetimes of 115 μsec and 1.05 msec. The former lifetime agrees with the 136-μsec lifetime measured by direct excitation of $^5D_1$ while monitoring fluorescence from the $^5D_1$ state. The 1.05-msec lifetime must then correspond to the $^5D_0$state.

b. Other centers. A number of other centers were observed in the excitation spectra (see Fig. 1) with transition intensities that ranged from 0.05% to 7% of the a1-site transitions. Typical spectral linewidths (Fig. 1) for the transitions of minority centers in the single crystal were 0.15–0.3 Å at 12 K. These narrow linewidths allowed reasonably selective excitation for many centers. Correlation of fluorescence spectra obtained by exciting each of the transitions in turn enabled assignment of most of the transitions to ten new sites labeled $b-k$.

Site-selective $^7F_0 \rightarrow {}^5D_1$ excitation spectra for all sites are included in Fig. 4. $^7F_0 \rightarrow {}^5D_1$ transition wavelengths for each center are included in Table III. Only four weak transitions marked with an asterisk in Fig. 1 were not assigned. Table III includes wavelengths of $^5D_0 \rightarrow {}^7F_1$and $^5D_0 \rightarrow {}^7F_2$ fluorescence transitions that can be used to produce site-selective excitation spectra for the new centers. As expected, the single-crystal spectra contained no evidence of Eu^{3+} centers in the Sr_2TiO_4 or $Sr_3Ti_2O_7$ phases.[41]

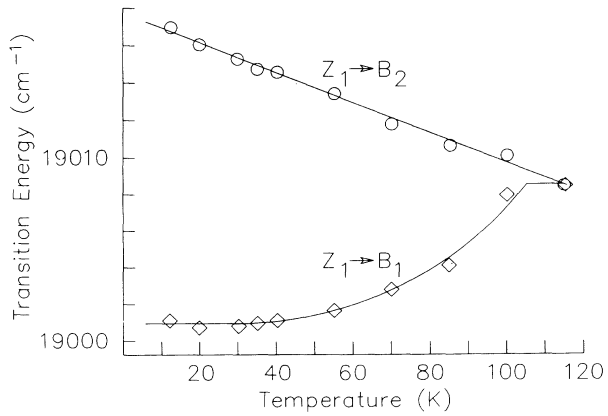

FIG. 7. Temperature dependence of the energies of the two a1-site $^7F_0 \rightarrow {}^5D_1$ transitions derived from the single-crystal excitation spectra monitoring total fluorescence.

In most spectra the $a-f$-center transitions dominated. Several site-selective fluorescence spectra of these centers are given in Fig. 5. The greater multiplicity of $^5D_2$ resulted in poorer site discrimination in the $^7F_0 \rightarrow {}^5D_2$ excitation spectra compared with $^7F_0 \rightarrow {}^5D_1$. The $a-d$ site-selective excitation spectra for $^7F_0 \rightarrow {}^5D_0$ and $^7F_0 \rightarrow {}^5D_2$ are given in Figs. 2 and 3. Despite the fact that only one electronic transition occurs per center, the $^7F_0 \rightarrow {}^5D_0$ excitation spectra were less useful, for survey purposes, than the $^7F_0 \rightarrow {}^5D_1$ spectra since electronic transitions of centers with a near inversion symmetry are relatively weak. The broad transitions dominating the total fluorescence $^7F_0 \rightarrow {}^5D_0$ excitation spectrum are vibronic transitions of the $a1$ center. Vibronics of the new centers are much weaker, relative to their zero-phonon electronic transitions, than the $a1$ center. If a center has cubic symmetry, electric dipole transitions are forbidden for the zero-phonon transition, but the vibronic transitions are allowed because of the removal of the cubic symmetry. One therefore expects that sites with near cubic symmetry might have relatively large vibronic features relative to the zero-phonon transition. The weakness of the vibronic transitions in the new centers then reflects their lower symmetry. $^5D_1$ energy levels are derivable from Table III for several new centers.

TABLE II. Energy levels (cm^{-1} in vacuum) of the $a1$ center in $SrTiO_3$:Eu^{3+} at 12 K derived from excitation and fluorescence spectra.

Manifold	Level number	Energy
$^5D_2$	3	21492.5
	2	21472.0
	1	21464.5
$^5D_1$	2	19016.9
	1	19001.1
$^5D_0$	1	17248.0
$^7F_6$	10	5723.0
	9	5471.0
	8	5420.5
	7	5156.0
	6	5143.0
	5	4986.5
	4	4959.0
	3	4942.5
	2	4927.0
	1	4887.5
$^7F_5$	8	4096.0
	7	4051.5
	6	3938.5
	5	3890.0
	4	3802.5
	3	3798.0
	2	3784.5
	1	3754.0
$^7F_4$	7	3135.8
	6	3084.4
	5	3047.4
	4	3012.5
	3	2770.2
	2	2633.7
	1	2583.4
$^7F_3$	5	1931.6
	4	1842.6
	3	1835.8
	2	1817.8
	1	1811.0
$^7F_2$	4	1033.5
	3	1003.4
	2	963.0
	1	946.3
$^7F_1$	2	329.5
	1	329.1
$^7F_0$	1	0

The spectra and energy levels reported here are those measured at 12 K. Like the $a1$ site, energy levels of each of the minority centers also varied with temperature. The lowest available temperature, 12 K, was used to characterize the crystal system as it gave the greatest energy-level separations and therefore the best spectral discrimination. At 77 K there was considerably more spectral overlap between centers.

Most of the centers had polarized emission and fluorescence transitions. In some cases the use of different polarization combinations enhanced the discrimination between sites. For example, it is difficult to discriminate between the transitions of the e and f sites because they are typically separated by only 0.025–0.065 nm for the $^5D_0 \rightarrow {}^7F_1$ and $^7F_2$ spectra. In these cases site discrimination can be improved by using the different polarization dependence of the absorption and fluorescence spectra. In these experiments we use the notation $x(a,b)z$, where x and z are the directions of laser and fluorescence propagation and a and b are the laser and fluorescence polarizations. The y and z laboratory axes are approximately aligned with crystalline $\langle 100 \rangle$ axes, but the third orthogonal crystal axis was not well defined for these experiments. Table IV gives relative intensities for the 12-K $^7F_0 \rightarrow {}^5D_1$ excitation transition at 527.109 and 527.088 nm for the e and f sites, respectively, when monitoring the strongest $^5D_0 \rightarrow {}^7F_1$ and $^5D_0 \rightarrow {}^7F_2$ transitions with each polarization for each of the sites. The optimum ratio of the e- and f-site excitation transition intensities is not always obtained by using a constant combination of input and output polarizations. When monitoring $^5D_0 \rightarrow {}^7F_1$, the discrimination between e and f sites is best optimized for the f site using $x(zx)z$ polarization and for e site using $x(yy)z$ polarization. Similarly, $x(zy)z$ and $x(yy)z$ polarizations are used to optimize discrimination of the e and f sites, respectively, when monitoring $^5D_0 \rightarrow {}^7F_2$. This technique of polarization-enhanced discrimination will be very important if defect quantification is required in future applications.

TABLE III. $^7F_0 \rightarrow {}^5D_1$ excitation transitions and the best emission transitions for monitoring individual site spectra (in nm).

Site	$^7F_0 \rightarrow {}^5D_1$ excitation	$^5D_0 \rightarrow {}^7F_1$ fluorescence	$^5D_0 \rightarrow {}^7F_2$ fluorescence
*a*1	526.140, 525.702	590.901	615.418
b	526.614, 526.227, 525.989	589.795	613.435
c	526.480, 526.323, 525.972	591.220	613.000
d	526.659, 526.310, 526.261	590.430	613.980
e	527.109, 526.494, 526.161	589.457	612.270
f	527.088, 526.444, 526.233	589.433	612.210
g	526.934, 526.410, 525.911	589.055	
h	528.708, 528.024, 527.946	591.385	619.465
i	528.588, 527.735	591.200	618.730
j	527.177, 526.582, 526.518	589.885	612.610
k	528.740, 528.131, 527.908	591.500	615.900
l	527.311, 527.301	590.585	

B. Polycrystalline $SrTiO_3$

$SrTiO_3$ was also prepared as polycrystalline ceramic pellets with Eu^{3+} concentrations of 0.01–0.2 mol%. The pellets were ground into powders and characterized by x-ray diffraction and laser excitation or fluorescence. The powders were normally examined after the calcining stage (see Sec. II) and again after various high-temperature sintering steps.

X-ray diffraction of samples after the initial calcining step showed that the powder was mostly $SrTiO_3$ phase, but typically contained a small component of rutile TiO_2 and a corresponding strontium-rich phase of either Sr_2TiO_4 or undissolved $SrCO_3$.

The total fluorescence $^7F_0 \rightarrow {}^5D_1$ excitation spectrum of calcined samples showed very broad *a*1-site transitions. For example, the 526.14-nm transition linewidth was typically 0.1–0.13 nm compared with the 0.018-nm width in the single crystal. In those calcined samples with a small Sr_2TiO_4-phase component, the transitions due to the *a*2 Eu^{3+} site in Sr_2TiO_4 (Ref. 41) were also observed in the total fluorescence excitation spectra. The samples before sintering also exhibited a broad excitation background in the total fluorescence $^7F_0 \rightarrow {}^5D_1$ excitation spectrum with an intensity of about 4–5% of the 526.14-nm peak. The $^5D_0$ fluorescence lifetime of this background was about 1 msec, consistent with assignment to Eu^{3+} emission. The minority centers seen in the single crystal could not be discriminated against this broad background.

Subjecting the calcined $SrTiO_3$ powders to a further high-temperature sintering step improved their quality considerably. X-ray diffraction of the best samples revealed that the excess TiO_2 and $SrCO_3$ or Sr_2TiO_4 had reacted to form single-phase $SrTiO_3$. The broad background of Eu^{3+} emission in the $^7F_0 \rightarrow {}^5D_1$ spectra was decreased by a factor of 5–10, transitions of the minority centers observed in the single-crystal experiments were resolved, and the *a*1-site transition linewidths decreased significantly. The degree of improvement depended on the conditions of the sintering process. Heating for 6 h at 900 °C did not produce significant improvement. Two treatments giving comparable, and significant improvements were (a) 52 h at 1050 °C and (b) 24 h at 1450 °C. Annealing a pellet a second time with the latter treatment gave a slight improvement. All sintering in this study was at ambient pressure in air.

There are differences between the single-crystal and polycrystalline sample spectra, as can be seen in Fig. 8 for the $^7F_0 \rightarrow {}^5D_1$ excitation spectrum (monitoring total fluorescence) of sintered polycrystalline $SrTiO_3$: 0.02 mol% Eu^{3+}. The *a*1 center's 526.14-nm transition has additional side structure at slightly longer wavelength and weak broad structure between the two main peaks. The nature of the structure has not been determined. Its occurrence seems somewhat irreproducible, but is typi-

TABLE IV. Polarized intensities for an *e*-center (527.109 nm) and an *f*-center (527.088 nm) $^7F_0 \rightarrow {}^5D_1$ excitation transitions monitoring various *e*- and *f*-center transitions. Intensities are separately normalized for the $^5D_0 \rightarrow {}^7F_1$ and $^5D_0 \rightarrow {}^7F_2$ cases.

	$^5D_0 \rightarrow {}^7F_1$ emission				$^5D_0 \rightarrow {}^7F_2$ emission			
	Monitor *e*-center (589.422 nm) excitation transition		Monitor *f*-center (589.457 nm) excitation transition		Monitor *e*-center (612.270 nm) excitation transition		Monitor *f*-center (612.210 nm) excitation transition	
Polarization	*e* center	*f* center	*e* center	*f* center	*e* center	*f* center	*e* center	*f* center
x(*zx*)*z*	8.4	9.3	~0	13.5	19.5	41.8	15.5	89.4
x(*zy*)*z*	52.1	30.9	27.9	49.8	100	~0	98.2	22.7
x(*yx*)*z*	7.4	10.2	5.9	12.6	14.5	20.5	11.8	47.3
x(*yy*)*z*	100	55.8	51.6	95.8	95.5	~0	83.6	13.6

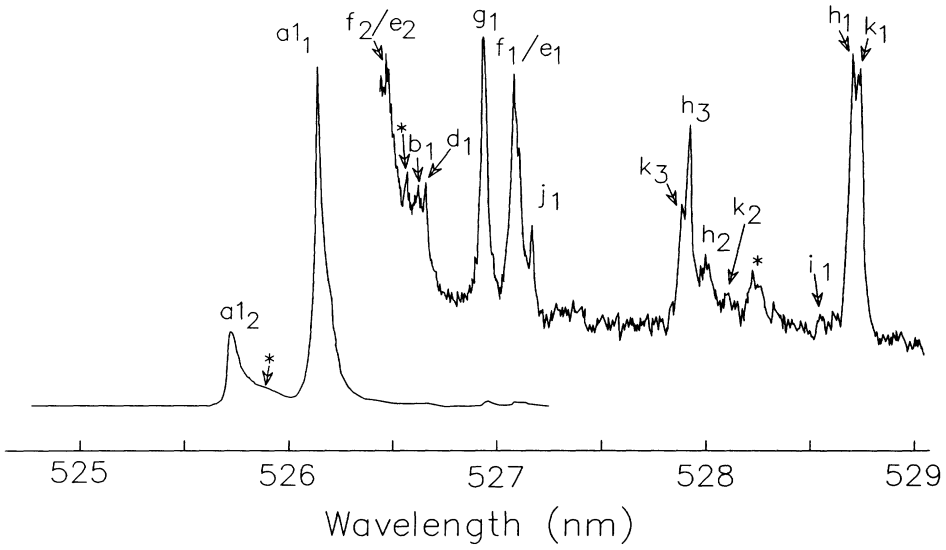

FIG. 8. $^7F_0 \rightarrow {}^5D_1$ excitation spectra of a polycrystalline $SrTiO_3$:0.02% Eu^{3+} sample monitoring total fluorescence with a temporal gate delay and width of 200 μsec/750 μsec. The asterisk indicates a real but unassigned peak.

cally reduced by high-temperature sintering. Collated spectra of several samples indicate that the intensity of the low-wavelength side structure increases with Eu^{3+} concentration.

Weaker transitions in Fig. 8 were confirmed, by site-selective laser excitation and fluorescence between several manifolds, to be those of the minority centers characterized in the single crystal. In all cases the linewidths were greater in the powders than in the single crystal, resulting in decreased discrimination between centers. The *e* and *f* sites, for example, were present, but not resolved in the powders. The temporal transients for each of the centers were the same when measured in the powders or the single crystal. In typical powders the minority-center peaks in the $^7F_0 \rightarrow {}^5D_1$ excitation spectra were 2–4 % as intense as the strongest $a1$-site transition (compared with about 7% in the single crystal).

The major differences between the single-crystal and polycrystalline spectra were the absence of the *c* site in the latter and the occurrence of a new site, labeled *l*, in the powders. (Figs. 4 and 8). The *g*, *h*, and *k* centers also had significantly greater relative intensity in the powders compared with the crystal. In some other cases the relative peak intensities of transitions in the site-selective spectra appeared different between powders and the single crystal. These differences were found, however, to be due to the more selective polarization combinations sampled in the single-crystal experiments.

The relative distribution of some minority centers was observed to change during storage at room temperature. The most significant change was a doubling of the *e* and *f* sites after 7 weeks and a small change in the *h* /*k*-site ratio.

Samples with 0.2 mol % Eu did not reveal any new sites compared to the 0.02% samples. Although total fluorescence intensity was greater, the relative distribution of minority centers was not significantly different. The lower-wavelength structure on the 526.14-nm $a1$-site transition was, however, relatively more intense.

A sample of 0.2 mol % Fe, 0.02% Eu was prepared to determine any correlation of a minority site to an Eu^{3+}-Fe^{3+} configuration. As no new centers were observed and the relative distribution of minority centers was not significantly changed, there is no evidence for such a center.

A recent study characterized the dominant Eu^{3+} centers in the Sr_2TiO_4 (a_2 site) and $Sr_3Ti_2O_7$ (a_3 and b_3 sites) phases.[41] Overlap between these transitions and the new $SrTiO_3$ minority centers was checked by direct comparison with Eu-doped single-phase Sr_2TiO_4 and $Sr_3Ti_2O_7$ samples. Two pairs of transitions were found to have near coincidence. First, the $Z1 \rightarrow B1$ transition of the $a2$ site is only 0.6 cm^{-1} higher than the $Z1 \rightarrow B1$ transition of the $a3$ site, which in turn is only 0.5 cm^{-1} higher than the $Z1 \rightarrow B1$ transition of the *g* site. In each case the fluorescence transitions and lifetimes are quite distinct, thereby enabling discrimination of $SrTiO_3$ minority centers from Sr_2TiO_4 and $Sr_3Ti_2O_7$ if materials of mixed phase were of interest.

It is probable that the cryogenically cooled polycrystalline materials were warmer than the single crystal. Section III A 3 *b* described the temperature dependence of the $a1$-site $^5D_1$ energy-level splittings in the single crystal. For the lowest attainable temperature ($\approx$12 K), the largest $^5D_1$-level separations were 15.8 and 15.2 cm^{-1} for the single crystal and powders, respectively. Although the single-crystal splitting did not vary significantly from day to day, the splitting in some powdered samples was observed to be as small as 13.8 cm^{-1}. Such variation is attributed to the limited thermal conductivity though contact points of grains of $SrTiO_3$. The variation depended on the grain size and powder-packing technique.

C. Other observations

1. Crystal coloration

An interesting effect was observed for laser excitation of the single-crystal and polycrystalline powders. Visual examination of the crystal for red-yellow-green laser excitation with Coumarin 481 or Rhodamine 6G dye with 100-μJ pulses (10-nsec duration) revealed a visible "black" line in the crystal of the approximate diameter of the laser beam. This line is best observed by blocking the pump beam and viewing the transmission through the crystal of a low-power white-light source. A surface coloration also occurred for excitation of the polycrystalline powders, but this was more difficult to probe. The visual clarity of the line increased with pump beam focusing, but did not depend on being resonant with a Eu^{3+} absorption. It did not appear to occur for blue excitation using the Coumarin 102 dye ($\sim$465 nm) used for the $^7F_0 \rightarrow {}^5D_2$ Eu^{3+} excitation experiments. The line was observed to form after 1–2 min and then to bleach after continuous laser excitation of approximately 5 min. When the pump laser was removed after the initial line formation, the line persisted with constant density (at 12 K) for at least 1 h (the longest period tested). The line could be removed by heating the sample to room temperature or by illuminating the sample with a 25-W tungsten lamp for approximately 1 min.

A possible mechanism for this coloration change is a photoinduced valence change of Ti^{4+} to Ti^{3+} which is optically active. Such a mechanism has been tentatively suggested to explain the similar observation of "colored" tracks formed in $KTiOPO_4$ nonlinear frequency-doubling crystals.[43] It is not obvious why the blue excitation does not form such a center when longer-wavelength excitation does. It is possible that a defect center present in the material is photoionized with excitation of specific visible absorption bands and the electrons released to the lattice are captured by the titanium ions.

2. Fluorescence bleaching

The intensity of fluorescence for $^7F_0 \rightarrow {}^5D_1$ resonant excitation of the $a1$ site in both the single-crystal and polycrystalline samples exhibited a bleaching behavior. Figure 9 shows the fluorescence intensity as a function of time for continuous laser excitation (10 Hz) on a fresh portion of sample for both the single crystal and a powder sample. The single-crystal fluorescence typically decayed by about 30% in the first 10 sec followed by a much slower decay ($\approx$10% in 5 min). After 5 min the signal was approximately constant. Spectra reported in this paper were recorded after the signal level had established a constant level.

Polycrystalline powder fluorescence typically decayed more slowly and by a greater fraction than the single-crystal fluorescence. The decay rate was longer for powders that were annealed at a high temperature for a shorter time (and having larger spectral linewidths). A typical sample decayed by 40% in 10 min then lost a further 15% over 30 min.

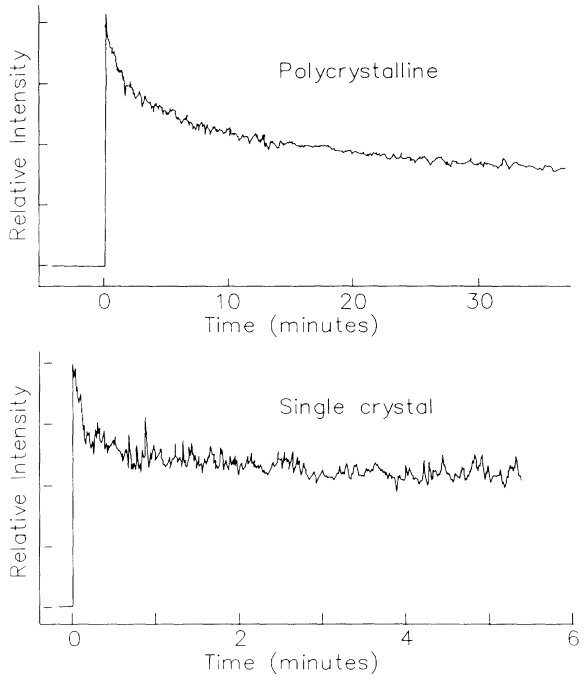

FIG. 9. Bleaching of the Eu^{3+} $a1$-site $^5D_0 \rightarrow {}^7F_1$ emission after excitation of the $^7F_0 \rightarrow {}^5D_1$ transition at 526.14 nm for a polycrystalline sample (top) and a single crystal (bottom).

The mechanism for the bleaching and the reason for the difference in rates between the powders and crystals is not known. At least two mechanisms are possible. First, the bleaching may be due to absorption of fluorescence by the black line formed with laser illumination. This mechanism seems unlikely as the time scales for formation and bleaching are different and, also, the fluorescence does not recover after the black line has bleached away again. Second, a photochemical or photophysical change in the environment of the Eu^{3+} ion in the $a1$ center would decrease its population. Such an environment change may result in a population increase of another center. Experiments using a weak probe laser may reveal the identity of such a center. A possible mechanism would be the capture of an electron by a Ti^{4+} ion. This would create sufficient perturbation of the Eu^{3+}-ion crystal-field symmetry to appear as fluorescence bleaching. This process, similar to the black-line formation, would not require the laser to be resonant on the Eu^{3+}-ion transitions. It may be possible to observe an increase in fluorescence intensity with time of some minority centers that involve a Ti^{3+} neighbor.

An alternative possibility is a europium capture of free electrons (photoionized from another defect) to give Eu^{2+} and therefore entirely different spectra. This mechanism would eliminate the need for charge compensation in $SrTiO_3$. Although Eu^{3+} is relatively easily reduced, other trivalent rare-earth ions are not. A search for fluorescence bleaching of other dopants in $SrTiO_3$ may aid confirmation of a specific bleaching mechanism.

3. Cr^{3+} spectroscopy

An unexpected fluorescence line was observed at 793.93 nm which had a very long fluorescence lifetime (>45 msec at 12 K). Detuning the laser revealed that this emission did not require resonance with any Eu^{3+} absorption. The excitation feature was very broad and exceeded the tuning range of the Coumarin 481 dye laser. The emission was identified as originating from Cr^{3+} on a Ti^{4+} site. A more detailed fluorescence scan revealed the vibronic structure characterized by Kim, Powell, and Wilson.[38] The crystal was nominally free of Cr^{3+} dopant, but this observation is consistent with previous observations of Cr^{3+} emission in most, nominally undoped, $SrTiO_3$ samples.[35,36]

A search was conducted for associated Cr^{3+}-Eu^{3+} centers. The proximity of the Eu^{3+} and Cr^{3+} ions should lead to $Eu^{3+}\rightarrow Cr^{3+}$ energy transfer. Laser excitation scans of the Eu^{3+} $^7F_0\rightarrow{}^5D_1$ region while monitoring $730\rightarrow780$ nm in 10-nm steps with a low-resolution monochromator ($\simeq$7-nm bandwidth) revealed no Eu^{3+} transitions which would confirm such a Cr^{3+}-Eu^{3+} center. As further confirmation, each of the known Eu^{3+} centers ($a-k$) were separately excited and the 700–800-nm fluorescence region was scanned. No evidence of fluorescence from a perturbed Cr^{3+} center associated with a known Eu^{3+} center was observed.

IV. DISCUSSION

A. $a1$ center

1. Structure

The $a1$ site is correlated to the cubic site reported by Weber and Schaufele.[1] Their spectra did not resolve all of the energy levels observed here because of their lower resolution and higher temperatures (77 K). Figure 7 shows that the $^7F_0\rightarrow{}^5D_1$ transitions are separated by 15.8 cm^{-1} at 12 K, but only 7.8 cm^{-1} at 77 K. Discrimination at 12 K is also aided by narrower spectral linewidths.

The collapse of energy-level splittings above 106 K confirms that the $a1$ center comprises an Eu^{3+} ion on a Sr^{2+}-ion site of cubic symmetry. Such a site is charge compensated remotely by a charged lattice defect. Energy-level splittings observed at lower temperature are attributed to a structural perturbation resulting from a rotation of the oxygen-ion octahedra close to the Eu^{3+} ions. This phase transition ($T_c=106$ K) and the rotation angles were characterized by Müller and Berlinger[2] using EPR as a probe of the local perturbation of Cr^{3+}- and Fe^{3+}-ion symmetry. The structural distortion creates a tetragonal symmetry at the probe-ion site. To our knowledge the $^7F_0\rightarrow{}^5D_1$ excitation spectra (Fig. 7) represent the best evidence of the effect of the phase transition on optical spectra. The continuous increase in Eu^{3+} perturbation with decreasing temperature indicates that the crystal structure contracts quite continuously with temperature.

Several features of the spectroscopy indicate that, even at the lowest temperatures, the $a1$ center is not strongly perturbed from cubic symmetry. First, the $^7F_0\rightarrow{}^5D_0$ electronic transitions are very weak and the $^5D_0$ lifetime is relatively long. Both electric and magnetic dipole mechanisms are forbidden for these transitions in a site with inversion symmetry. In contrast, the ratio of the $^7F_0\rightarrow{}^5D_0$ electronic transition to the $^7F_0\rightarrow{}^5D_1$ transition is much larger in the lower-symmetry Eu^{3+} sites of the Sr_2TiO_4 and $Sr_3Ti_2O_7$ phases and the minority centers of $SrTiO_3$ than that observed for the $a1$ site. Second, the crystal-field splittings of most $a1$-center manifolds are small. For example, the 15.8-cm^{-1} splitting of $^5D_1$ compares to 29.5 and 36 cm^{-1} for the $a2$ and $a3$ centers, respectively.[41]

2. Linewidths

The broad linewidths of $a1$-site transitions in powders, compared to the single crystal, are an indication of disorder. This disorder may be structural disorder at an atomic level or may be due to variation in the temperature of different grains of powder comprising the pressed spectroscopic sample. The linewidths usually decreased with prolonged high-temperature annealing. Heating provides the ion mobility required to improve the microscopic integrity of the sample and may also enable the growth of larger grains. Either effect may account for the line narrowing. Poorly sintered powders typically had asymmetrically broadened transitions with spectral structure, for example, located between the $^7F_0\rightarrow{}^5D_1$ $a1$-site excitation transitions. As proposed in a previous paper,[41] this structure may be the result of temperature inhomogeneities within the conductively cooled polycrystalline sample. Differences in temperature given different positions for $a1$-site transitions, as can be seen from Fig. 7. The distribution of temperatures gives a distribution of level positions responsible for the band.

B. Minority centers

None of the minority centers, $b-l$, have previously been reported. The differences in spectra of the 11 centers are indicative of distinct local perturbations of the environment of the Eu^{3+} ion. As the charge on the Eu^{3+} ion differs from the Sr^{2+} site it occupies, a charged species may associate with the Eu^{3+} ion to give a neutral center. The multitude of centers indicates that charge compensation may be provided by several different species located on various distinct lattice positions.

An unusual effect is expected for $SrTiO_3$ because of the oxygen octahedra rotation associated with the 106-K cubic-to-tetragonal phase transition. If the charge compensation is local to the Eu^{3+}, each distinct Eu^{3+} center in the cubic phase may be observed as two distinct centers in the lower-temperature tetragonal phase. The local axis defined by the charge compensation relative to Eu^{3+} in the center can have different inequivalent orientations with respect to the bulk tetragonal (100) axis that develops at low temperature, and so new sites will form. Therefore some of the centers $b-l$ observed at low temperature may correspond to each other in the cubic

phase. Unfortunately, the reduction of fluorescence intensity, the thermally induced transition broadening, and the overall reduction of transition separation and discrimination prevented any direct confirmation of center equivalence above 100 K. However, any combination of centers which differ only in orientation should always maintain constant relative intensities at low temperature. Comparison of the spectra of several powders and the single crystal revealed that the (b,d), (e,f), and (h,k) site pairs may represent examples of such orientation combinations. A detailed kinetic study, in which charge-compensating species are rearranged, should confirm all such related sets of centers. Since the $a1$ center does not have a local-charge compensation, the phase transition does not create inequivalent centers for the distantly compensated site.

The specific local configurations of the minority centers discovered in this study are unknown. As the tenfold increase in Eu^{3+} concentration from 0.02% did not result in the enhancement of any particular center, it is unlikely the centers comprise Eu^{3+}-ion clusters. Trivalent metal ions such as Fe^{3+}, Al^{3+}, and Cr^{3+} occupying a Ti^{4+}-ion site next to a Eu^{3+} ion would result in an electrically neutral center with a very distinct, perturbed, spectrum. Deliberate doping with 0.2% Fe^{3+} did not, however, enhance a particular center. Although the single crystal exhibited emission from a trace presence of Cr^{3+} on a Ti^{4+} site, a detailed search suggested that none of the minority centers are due to an Eu^{3+}-Cr^{3+} combination. Since the same centers (except for c and l) were observed with comparable intensity in both the single crystal and many powders (made from two independent sources of Ti^{4+} ions), it is unlikely that the centers are the result of specific accidental contamination of starting materials.

The $^5D_1$ energy-level splittings of several of the sites (derivable from Table III) are considerably greater than that of the $a1$ center, and the manifold is split into three components in most cases. The $^5D_1$-manifold barycenters of the h, i, j, k, and l centers are also significantly shifted from the $a1$ center. These observations indicate significant perturbation of the Eu^{3+} ion from the remotely charge-compensated $a1$-center symmetry and are consistent with local-charge compensation.

The most probable intrinsic defects in $SrTiO_3$ are negatively charged strontium vacancies (V''_{Sr}), trivalent titanium (Ti'_{Ti}), and positively charged oxygen vacancies ($V^{\cdot\cdot}_{O}$). Other workers have verified the existence of (Fe'_{Ti}-$V^{\cdot\cdot}_{O}$) charge-compensated defects.[33] In the current study, however, $V^{\cdot\cdot}_{O}$ are unlikely to associate with Eu^{3+} ($Eu^{\cdot}_{Sr}$) as both defects have positive charge. The 11 minority centers therefore probably comprise various locally charge-compensated configurations involving V''_{Sr} and Ti'_{Ti}. Associated $Eu^{\cdot}_{Sr}$-V''_{Sr} centers were recently proposed to account for minority centers in Sr_2TiO_4.[41] Several observations in the $SrTiO_3$ experiments are consistent with the formation of Ti^{3+}, which may provide charge compensation. First, relative site populations change during storage periods. Room-temperature ion migration is unlikely for such a closely packed lattice. Ti^{4+}-ion capture of migrating electrons is more likely. Centers involving Ti^{3+} charge compensation would grow with time at the expense of the $a1$-site population. Second, the black-line formation indicates that electrons can be released from electron traps by photoexcitation. These electrons are then trapped by a different species. Finally, the $a1$-center fluorescence bleaching is consistent with electron trapping by Ti^{4+} creating a locally compensated environment and a decreased $a1$-site population. Although this study has demonstrated the existence and importance of local-charge compensation for Eu^{3+}, further experiments are required to determine the exact local configurations of the minority centers.

V. CONCLUSIONS

Laser excitation and fluorescence spectra show that Eu^{3+} ions form a number of centers in $SrTiO_3$. Although a center with distant-charge compensation dominates, at least 11 other centers with local-charge compensation also exist. This observation is an important step toward the understanding and ability to probe the microscopic defect chemistry of $SrTiO_3$. The exact charge-compensating configurations of the minority centers are not known, but the migration of carriers observed suggests that Ti^{3+}-ion charge compensation may be important. Strontium vacancies are also expected to provide compensation. Future experiments, such as varying the oxygen fugacity to control intrinsic defect populations, will help to identify configurations.

Two unusual observations in the $SrTiO_3$:Eu^{3+} system are particularly interesting. First, fluorescence bleaching and black-line formation indicate that photoinduced electron injection plays an important role in the microscopic defect chemistry. Second, the Eu^{3+} spectroscopy strongly reflects the effect of the 106-K structural phase transition of $SrTiO_3$.

ACKNOWLEDGMENT

This research was supported by the National Science Foundation under Grant No. DMR-8815398.

*Present address: Los Alamos National Laboratory, Mail Stop J564, Los Alamos, NM 87545.

[1]M. J. Weber and R. F. Schaufele, Phys. Rev. **138**, A1544 (1965).
[2]K. A. Müller and W. Berlinger, Phys. Rev. Lett. **26**, 13 (1971).
[3]R. J. D. Tilley, J. Solid State Chem. **21**, 293 (1977).
[4]K. A. Müller and W. Berlinger, Phys. Rev. B **34**, 6130 (1986).
[5]J. F. Schooley, W. R. Hosler, and M. L. Cohen, Phys. Rev. Lett. **12**, 474 (1964).
[6]T. Feng, Phys. Rev. B **25**, 627 (1982).
[7]B. U. Faughnan, Phys. Rev. B **4**, 3623 (1971).
[8]I. Burn and S. Nierman, J. Mater. Sci. **17**, 3510 (1982).

[9]T. Tschudi, A. Herden, J. Goltz, H. Klumb, F. Laeri, and J. Albers, IEEE J. Quantum Electron. **QE-22**, 1493 (1986).
[10]K. A. Müller, W. Berlinger, and J. Albers, Phys. Rev. B **32**, 5837 (1985).
[11]R. A. Serway, W. Berlinger, K. A. Müller, and R. W. Collins, Phys. Rev. B **16**, 4761 (1977).
[12]H. M. Al-Allak, A. W. Brinkman, G. J. Russell, and J. Woods, J. Appl. Phys. **63**, 4530 (1988).
[13]J. G. Bednorz and K. A. Müller, Z. Phys. B **64**, 189 (1986).
[14]N. H. Chan and D. M. Smyth, J. Electrochem. Soc. **123**, 1584 (1976).
[15]D. M. Smyth, J. Solid State Chem. **16**, 73 (1976).
[16]D. M. Smyth, J. Solid State Chem. **20**, 359 (1977).
[17]N. H. Chan, R. K. Sharma, and D. M. Smyth, J. Electrochem. Soc. **128**, 1762 (1981).
[18]U. Balachandran and N. G. Eror, J. Mater. Sci. **17**, 2133 (1981).
[19]N. G. Eror and U. Balachandran, J. Solid State Chem. **40**, 85 (1981).
[20]U. Balachandran and N. G. Eror, J. Solid State Chem. **39**, 351 (1981).
[21]U. Balachandran and N. G. Eror, J. Electrochem. Soc. **129**, 1021 (1982).
[22]N. G. Eror and U. Balachandran, J. Am. Ceram. Soc. **65**, 426 (1982).
[23]B. Odekirk, U. Balachandran, N. G. Eror, and J. S. Blakemore, Commun. Am. Ceram. Soc. **66**, C22 (1983).
[24]B. F. Flandermeyer, A. K. Agarwal, H. U. Anderson, and M. N. Nasrallah, J. Mater. Sci. **19**, 2593 (1984).
[25]B. F. Flandermeyer, M. N. Nasrallah, D. H. Sparlin, and H. U. Anderson, in *Transport in Nonstoichiometric Compounds,* Vol. 129 of *NATO Advanced Study Institute, Series B: Physics,* edited by George Sinkovich and V. S. Stubican (Plenum, New York, 1985).
[26]D. R. Tallant and J. C. Wright, J. Chem. Phys. **63**, 2074 (1975).
[27]J. C. Wright, Cryst. Latt. Def. and Amorph. Mat. **12**, 505 (1985), and references therein.
[28]M. J. Weber and R. F. Schaufele, J. Chem. Phys. **43**, 1702 (1965).
[29]H. Yamamoto, S. Makishima, and S. Shionoya, J. Phys. Soc. Jpn. **23**, 1321 (1967).
[30]K. A. Müller, Phys. Rev. Lett. **2**, 341 (1959).
[31]K. W. Blazey, J. M. Cabrera, and K. A. Müller, Solid State Commun. **45**, 903 (1983).
[32]E. Siegel and K. A. Müller, Phys. Rev. B **19**, 109 (1979).
[33]E. S. Kirkpatrick, K. A. Müller, and R. S. Rubins, Phys. Rev. **135**, A86 (1964).
[34]L. Rimi and G. A. Mars, Phys. Rev. **127**, 702 (1962).
[35]L. Grabner, Phys. Rev. **177**, 1315 (1969).
[36]S. E. Stokowski and A. L. Schawlow, Phys. Rev. **178**, 457 (1969).
[37]S. E. Stokowski and A. L. Schawlow, Phys. Rev. **178**, 464 (1969).
[38]Q. Kim, R. C. Powell, and T. M. Wilson, Solid State Commun. **14**, 541 (1974).
[39]A. Mackor and G. Blasse, Chem. Phys. Lett. **77**, 6 (1981).
[40]M. Pechini, U.S. Patent No. 3 330 697 (1967).
[41]N. J. Cockroft, S. H. Lee, and J. C. Wright, Phys. Rev. B **44**, 4117 (1991).
[42]G. H. Dieke, in *Spectra and Energy Levels of Rare Earth Ions in Crystals,* edited by H. M. Crosswhite and H. Crosswhite (Interscience, New York, 1968).
[43]J. C. Jacco, D. R. Rockafellow, and E. A. Teppo, Opt. Lett. **16**, 1307 (1991).